BIOCHEMISTRY
including biophysical chemistry & molecular biology

Article

pubs.acs.org/biochemistry

Allosteric Activation via Kinetic Control: Potassium Accelerates a Conformational Change in IMP Dehydrogenase

Thomas V. Riera,[†,#] Lianqing Zheng,[∥] Helen R. Josephine,[‡] Donghong Min,[∥] Wei Yang,*[,∥,⊥] and Lizbeth Hedstrom*[,‡,§]

[†]Graduate Program in Biochemistry, [‡]Department of Biology, and [§]Department of Chemistry, Brandeis University, 415 South St., MS 009, Waltham, Massachusetts 02454, United States

[∥]Institute of Molecular Biophysics and [⊥]Department of Chemistry and Biochemistry, Florida State University, Tallahassee, Florida 32306, United States

Supporting Information

ABSTRACT: Allosteric activators are generally believed to shift the equilibrium distribution of enzyme conformations to favor a catalytically productive structure; the kinetics of conformational exchange is seldom addressed. Several observations suggested that the usual allosteric mechanism might not apply to the activation of IMP dehydrogenase (IMPDH) by monovalent cations. Therefore, we investigated the mechanism of K^+ activation in IMPDH by delineating the kinetic mechanism in the absence of monovalent cations. Surprisingly, the K^+ dependence of k_{cat} derives from the rate of flap closure, which increases by ≥65-fold in the presence of K^+. We performed both alchemical free energy simulations and potential of mean force calculations using the orthogonal space random walk strategy to computationally analyze how K^+ accelerates this conformational change. The simulations recapitulate the preference of IMPDH for K^+, validating the computational models. When K^+ is replaced with a dummy ion, the residues of the K^+ binding site relax into ordered secondary structure, creating a barrier to conformational exchange. K^+ mobilizes these residues by providing alternate interactions for the main chain carbonyls. Potential of mean force calculations indicate that K^+ changes the shape of the energy well, shrinking the reaction coordinate by shifting the closed conformation toward the open state. This work suggests that allosteric regulation can be under kinetic as well as thermodynamic control.

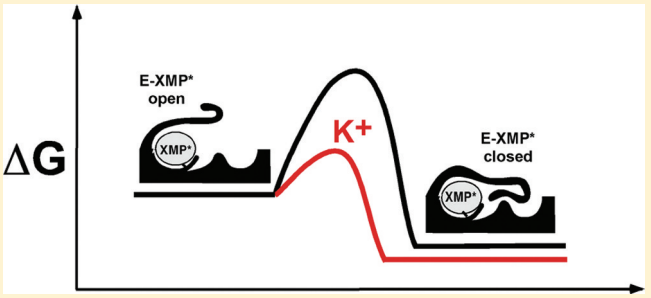

Virtually every cellular process is regulated by the allosteric control of protein function, in which the binding of an effector ligand modulates the function of a second site. How effector binding changes the properties of a distal binding site is a long-standing problem in biochemistry.[1−3] Textbook models explain allostery in terms of shifting the equilibrium between active and inactive protein conformations. For example, many enzymes are activated by monovalent cations such as K^+; cation binding is believed to stabilize a conformation that has a higher affinity for substrates or is more proficient in catalyzing the chemical transformation[4] (Figure 1A). Recent treatments of allostery emphasize that proteins exist in conformational ensembles, but the underlying effector-induced shift in the distribution of conformations still applies.[5−8] An alternative model, termed dynamic allostery, posits that an effector changes the distribution of substates within a single conformation, and an example of this phenomenon is also known (Figure 1B).[9−11] These models presume that the conformational ensemble is at equilibrium; recast in the language of a chemical reaction coordinate, these models invoke changes in ground state conformations and are therefore examples of thermodynamic control. The interconversion of conformations is generally assumed to be rapid and

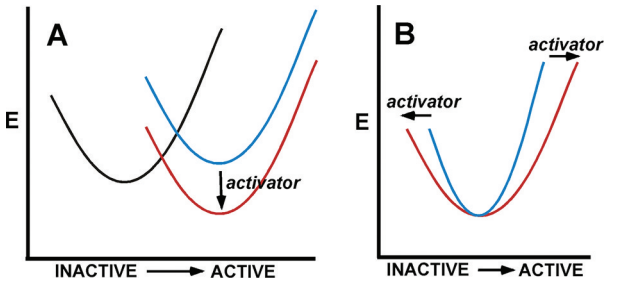

Figure 1. Allosteric mechanisms. While it is recognized that proteins exist as conformational ensembles, only two states are depicted to emphasize the differences in the panels. (A) The activator stabilizes the active conformation. (B) The activator changes the fluctuations within a single conformation. In this example, activation involves increasing conformational fluctuations, as has been observed in catabolite activator protein.[10] In principle, activation could also occur by decreasing conformational fluctuations.

Received: May 20, 2011
Revised: August 25, 2011
Published: August 26, 2011

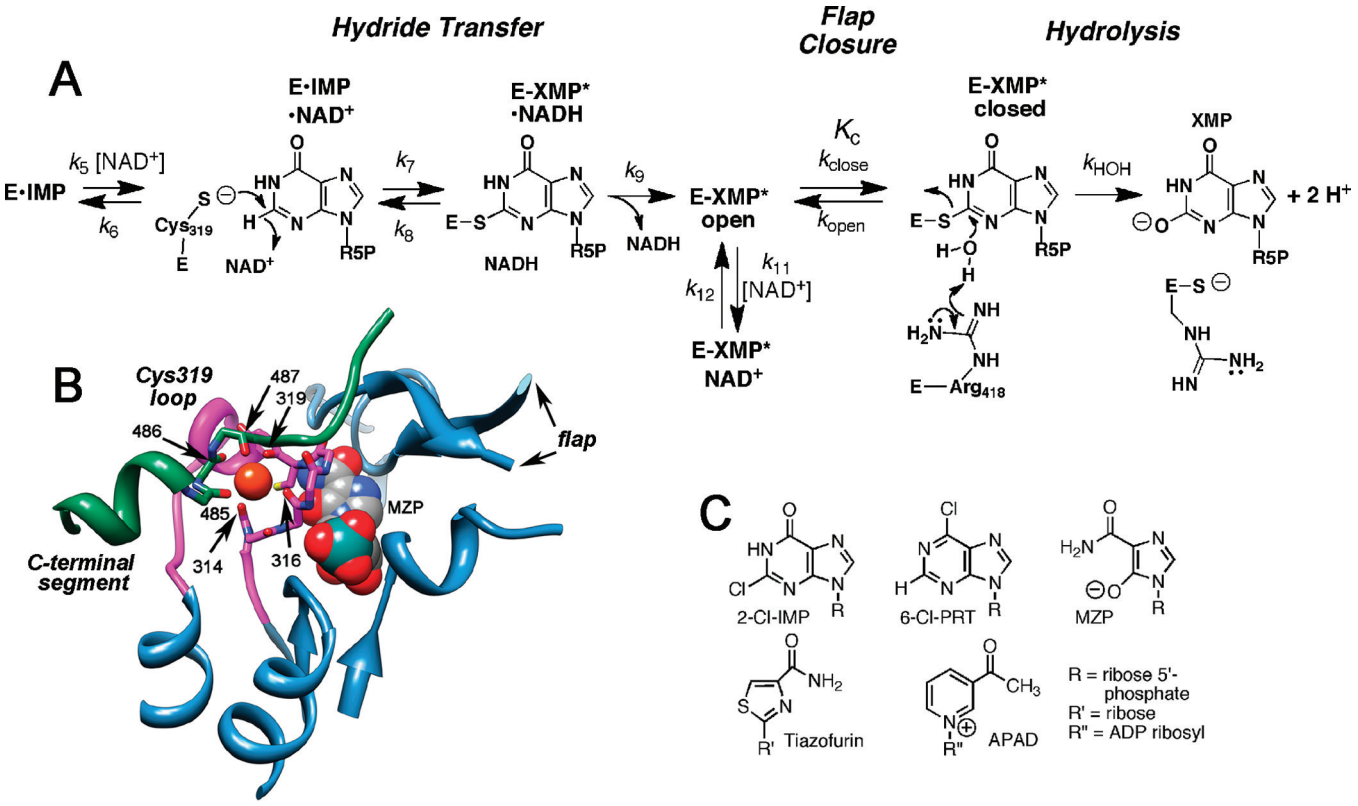

Figure 2. IMPDH mechanism and structure. (A) Mechanism of the IMPDH reaction. R5P, ribose-5′-monophospate. (B) The conserved K^+ site in the E·MZP complex of *Tf*IMPDH (PDB accession number 1PVN[15]). The Cys loop is shown in magenta, and the C-terminal helix from the adjacent subunit is shown in green. The K^+ binding site is formed by the main chain carbonyl oxygens of Gly314, Gly316, the catalytic Cys319, Glu485, Gly486, and Gly487. This panel was produced with UCSF Chimera.[53] (C) Structures of compounds. MZP, mizoribine monophosphate; APAD, acetylpyridine adenine dinucleotide; R′, ribose; R″, ADP-ribosyl.

inconsequential. Therefore, the impact of allosteric effectors on the rates of conformational changes has usually been ignored.

At first glance, the activation of IMP dehydrogenase (IMPDH) by K^+ appears to be a textbook example of allosteric activation.[4] This enzyme catalyzes the conversion of IMP to XMP with the concomitant reduction of NADH (Figure 2A).[12] K^+ increases IMPDH activity by ∼100-fold.[12] Several X-ray crystal structures of IMPDH identified a conserved K^+ binding site formed by six main chain carbonyls: three from the loop that contains the catalytic Cys319 and three from an α helix in the C-terminal segment of the adjacent subunit (Gly314, Gly316, the catalytic Cys319, Glu485′, Gly486′, and Gly487′, where the prime denotes residue from the neighboring subunit, Figure 2B; *Tritrichomonas foetus* IMPDH (*Tf*IMPDH) numbering will be used throughout[13−15]). Thus, K^+ seems ideally positioned to promote substrate binding and/or the rate of the chemical transformations.

Several observations suggest that K^+ does not simply stabilize an active enzyme conformation. First, K^+ does not increase the affinity of substrates.[16,17] Second, K^+ does not accelerate the IMPDH-catalyzed hydrolysis of 2-Cl-IMP to XMP[16,17] (substrate/inhibitor structures are shown in Figure 2C). Third, 6-Cl-purine ribotide (6-Cl-PRT) inactivates IMPDH by forming a covalent adduct with Cys319 at the 6-position of the purine ring. Adduct formation requires distortion of the Cys319 loop, which disrupts the K^+ site,[18] yet K^+ does not protect against inactivation.[16,19] Lastly, the K^+ site is disrupted in many structures of IMPDH complexes.[18,20−22] If these structures reflect intermediates of the catalytic cycle as is believed, then K^+ must have a transient association with the enzyme.[12,14,23]

IMPDH has a complicated catalytic cycle that involves two different chemical transformations and several conformational changes (Figure 2A).[12,23] Ten X-ray crystal structures of *Tf*IMPDH have been solved in complex with various substrates and inhibitors.[14,15,20−22] These structures suggest the following reaction sequence, which is generally corroborated by structures of IMPDHs from other sources and additional biochemical experiments: In the absence of substrates, the Cys319 loop (residues 313−328), the flap (residues 412−431), and the C-terminal segment (residues 481−503) are disordered. The binding of IMP and NAD^+ orders these regions, although part of the flap and C-terminal segment remain disordered.[14,24,25] The structures suggest that K^+ is not bound in the E·IMP·NAD^+ complex. The reaction proceeds with the attack of Cys319 on the C2 position of IMP. Hydride is transferred to NAD^+, producing NADH and the covalent intermediate E-XMP*. Monovalent cations are observed in the structures of E-XMP* and IMP analogues MZP and RVP.[13,15] These two inhibitors lack the six-membered ring of purine bases, which permits the Cys319 loop to assume the same conformation as in E-XMP*. These observations suggest that K^+ binds after E-XMP* forms.

A conformational change is required for the hydrolysis of E-XMP*. NADH departs, allowing the flap to fold into the vacant dinucleotide site. This conformational change brings the catalytic base Arg418 into the active site, causing the hydrolysis of E-XMP* to yield XMP. Alternatively, NAD^+ can bind in the

dx.doi.org/10.1021/bi200785s | *Biochemistry* 2011, 50, 8508−8518

vacant dinucleotide site, forming a dead end complex. Recent work suggests that the Cys319 loop has different conformations in E-XMP*$_{open}$ and E-XMP*$_{closed}$.[26] Therefore, the conformation of the Cys319 loop gates flap closure.

While the X-ray crystal structures suggest that K^+ only binds to E-XMP* complexes, steady-state kinetic experiments indicate that K^+ is required for NAD^+ binding in *Aerobacter aerogenes* and *Escherichia coli* IMPDHs[19,27] and must occur before either substrate binds in human IMPDH type 2.[17] These observations cast doubt on the catalytic relevance of many IMPDH crystal structures. Therefore, we decided to examine the effect of K^+ on individual steps in the IMPDH reaction. Although *Tf* IMPDH is the best characterized IMPDH, this enzyme is a poor system to investigate the mechanism of K^+ activation because it contains a second monovalent cation binding site not found in other IMPDHs.[14,20] Fortunately, *Cryptosporidium parvum* IMPDH (*Cp*IMPDH) contains only the conserved monovalent cation binding site.[28] The kinetic mechanism of *Cp*IMPDH has been characterized in detail in the presence of K^+ and is typical of IMPDHs:[29] substrates add randomly and hydride transfer is fast. High concentrations of NAD^+ inhibit the reaction by trapping E-XMP* (Figure 2A). A solvent isotope effect is observed on k_{cat} (SIE = 2.6), which indicates that the conformational change is fast and the attack of water is rate-limiting.

Our experiments show that K^+ is present throughout the catalytic cycle but has the biggest effect on the rate of flap closure. Simulations reveal that K^+ mobilizes residues on the Cys319 loop by providing alternative interactions for the main chain carbonyl oxygens. Thus, K^+ effectively acts as the ball-and-socket joint that facilitates the conformational changes required for completion of the catalytic cycle.

MATERIALS AND METHODS

General. The sodium salts of XMP, NADH, and ADP were converted into $TrisH^+$ salts by cation exchange using Dowex 50Wx4 resin. All other substrates, products, and ligands were used in their free acid forms. [8-^{14}C]-IMP (Moravek Biochemicals, Inc.) was used as the ditriethylammonium salt. Tiazofurin was obtained from the Open Chemical Repository at the NCI Developmental Therapeutics Program. Low-conductivity D_2O and DCl were purchased from Cambridge Isotope Laboratories, Inc. *Cp*IMPDH was expressed and purified as previously described.[30]

Steady-State Kinetics. Assays in the absence of monovalent cation used tetramethylammonium chloride or Tris-Cl to maintain ionic strength. Standard IMPDH assays were performed at 25 °C in assay buffer (280 mM Tris-Cl, pH 8.0, and 1 mM DTT) with 100−200 nM enzyme. NADH or APADH production was monitored spectrophotometrically at 340 nm (NADH, ε = 6.22 mM^{-1} cm^{-1}) or 363 nm (APADH, ε = 9.1 mM^{-1} cm^{-1}). Initial velocities were fit by SigmaPlot (Systat Software Inc.) using either the Michaelis−Menten equation (eq 1) or an equation for uncompetitive substrate inhibition (eq 2)

$$v = V_m[S]/(K_M + [S]) \quad (1)$$

$$v = V_m/(1 + (K_M/[S]) + ([S]/K_{ii})) \quad (2)$$

where v is the initial velocity, V_m is the maximal velocity, K_M is the Michaelis constant for substrate (S), and K_{ii} is the inhibition constant for S.

Cation Activation of CpIMPDH. Cation activation of IMPDH activity was measured in 50 mM Tris-Cl, pH 8.0, 1 mM DTT, 500 μM IMP, and 500 μM NAD^+ at 25 °C. Final enzyme concentrations of 40−100 nM were used. The chloride salt of each cation was used. Ionic strength (and Cl^- concentration) was maintained with tetramethylammonium chloride (TMA·Cl), which neither activates *Cp*IMPDH nor inhibits K^+ activation (data not shown). The fits of K^+ and NH_4^+ activation are by eqs 3 and 4, respectively:

$$v/E = \{V_{max}[A]/(K_A + [A])\} + k_{basal} \quad (3)$$

$$v/E = \{V_{max}/(1 + (K_A/[A]) + ([A]/K_{ii}))\} + k_{basal} \quad (4)$$

where k_{max} is the maximal rate, K_A is the concentration of activator (A) at $^1/_2k_{max}$, K_{ii} is the uncompetitive inhibition constant for activator, and k_{basal} is the initial velocity in the absence of cation.

Solvent Deuterium Isotope Effects. Assay buffer was prepared in either H_2O or D_2O. The pH meter readings in D_2O were adjusted by adding 0.4. Initial velocities were measured for varying dinucleotide in assay buffer with 500 μM IMP at 25 °C.

Multiple Inhibitor Studies with Tiazofurin and ADP. Initial velocities were measured in the presence of varying tiazofurin and ADP. Assay conditions were 200 nM *Cp*IMPDH, 500 μM IMP, 200 μM APAD, 281 mM Tris-Cl, pH 8.0, and 1 mM DTT. The interaction constant aα was determined by fitting the data with the multiple inhibitor equation as previously described.[31]

Trapping E-XMP*. Accumulation of the covalent E-XMP* complex was measured from reactions with 100 μM [8-^{14}C]-IMP, 2 μM *Cp*IMPDH, and 1.25 mM NAD^+ or 2.5 mM $APAD^+$ in assay buffer at 25 °C. Reactions were quenched with cold trichloroacetic acid to a final concentration of 10% during the steady state. Protein was captured on 0.45 mm HA nitrocellulose filters and washed with cold 10% TCA. Radioactivity was measured by scintillation counting. Control reactions lacked enzyme or dinucleotide.

Molecular Dynamics Free Energy Simulations. The CHARMM 27 parameters were utilized in this study. The parameters of all the ions were based on the existing optimized CHARMM force field.[32] In each alchemical transition for relative binding affinity calculations, the scaling parameter λ was used to switch the state from one cation to another; for example, λ = 0 for Na^+ and λ = 1 for K^+. In the calculation of the absolute binding affinity of K^+, the state of λ = 0 represents a dummy particle that does not have any interactions with the other atoms but is restrained to the carbonyl oxygen atom of residue 316 with the reference distance set as 2.81 Å and with the force constant set as 100 kcal/(mol Å^2). In addition, an angle restraint was employed on the dummy−carbonyl oxygen−carbonyl carbon with the reference angle set as 132.0° and the force constant set as 10 kcal/(mol rad^2); a dihedral restraint was employed on the dummy−carbonyl oxygen−carbonyl carbon−amide nitrogen (residue 317) angle with the reference angle set as −110.0° and the force constant set as 10 kcal/(mol rad^2). The free energy contribution based on this restraint setup can be analytically estimated[33] via the following ansatz:

$$\Delta G_{\text{restraint}}([\text{ion}]) = RT \ln\left[\frac{8\pi^2 V^\circ}{r_B^2 \sin\theta_A}\frac{(K_B K_A K_D)^{1/2}}{(2\pi RT)^{3/2}}\frac{(1\text{ M})}{[\text{ion}]}\right] \quad (5)$$

where K_B, K_A, and K_D represent the force constants of the restraining bond, angle, and dihedral angle, respectively; r_B stands for the reference distance of the restraining bond; θ stands for the reference value of the restraining angle; [ion] stands for the ion concentration (molarity); V° denotes 1660 Å^3; and R is the ideal gas constant.

In this model, the soft-core form of the nonbonded interaction switching was used with the shifting parameter set as 6 Å^2 and the particle-mesh Ewald (PME) method was applied to take care of the long-range Coulombic interactions, whereas the short-range interaction was switched starting at 10 Å and totally off at 12 Å. The temperature was set as 300 K, which was kept constant via the Langevin thermostat. Molecular dynamics simulations were integrated via a time-step of 1 fs.

All the free energy simulations were performed based on the orthogonal space random walk (OSRW) method.[34,35] The OSRW method is a generalized ensemble simulation technique which requires adaptive updates of the biasing energy terms to accelerate related molecular motions. An OSRW simulation requires two recursion components: a recursion kernel and a recursion slave to respectively update two biasing energy terms: the orthogonal space biasing term and the order parameter space biasing term. In the present implementation, the recursion kernel, which updates the orthogonal space biasing term, is based on the metadynamics method.[36] In the metadynamics recursion kernel, the height and width of the Gaussian function were set as 0.01 and 4 kcal/mol, respectively; the orthogonal space biasing potential was updated every 10 time steps, and the order parameter space biasing potential was updated every 100 time steps. The order parameter space biasing term, which depends on the orthogonal space biasing term, is estimated via the thermodynamic integration based recursion slave procedure. Free energy convergence is obtained with the fluctuation range of the estimated free energy values reaching about 0.1 kcal/mol in 500 ps simulations.

Potential of mean force calculations were also based on the orthogonal space random walk method with the same general simulation setup as described above. The average of the distances between each C-α atom in the flap (residues 302–320 in *Cp*IMPDH numbering) and the center of the XMP* base atoms is employed as the collective variable. In the generated free energy profiles, the state with the collective variable of 12 Å was set as the reference state with the free energy value of zero. Thereby, the free energy profiles corresponding to the states in the presence and absence of K^+ cannot be directly compared.

RESULTS

Influence of Monovalent Cations on CpIMPDH Activity. The activation of *Cp*IMPDH by monovalent cations is typical for IMPDHs. Both K^+ and NH_4^+ increased the activity of *Cp*IMPDH by 40-fold (Figure 3).[12] The activation properties of K^+ and NH_4^+ were nearly identical, as expected given the similar sizes of these two cations and as observed in other IMPDHs.[12] In contrast, Na^+ had little effect on the *Cp*IMPDH reaction. Li^+, Mg^{2+}, and Ca^{2+} inhibited K^+ activation but did not block the basal reaction (Figure S1).

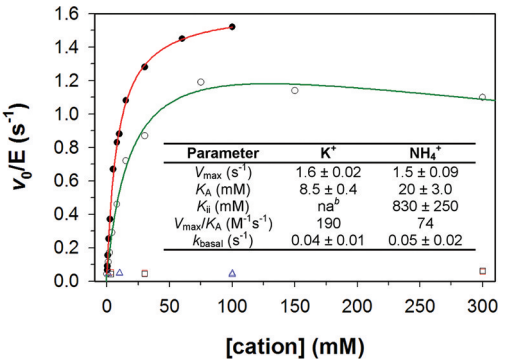

Figure 3. Cation activation of the *Cp*IMPDH reaction. K^+ (●), NH_4^+ (○), Na^+ (□), Li^+ (red □), Mg^{2+} (△), and Ca^{2+} (blue △). The fits of K^+ and NH_4^+ activation are by eq 3 and eq 4, respectively. Assays were performed in 50 mM Tris-Cl, pH 8.0, 1 mM DTT, 500 μM IMP, and 500 μM NAD^+ at 25 °C. [b]Not applicable. V_{max} is the apparent maximal rate, K_A is the apparent affinity of the monovalent cation, and K_{ii} is the inhibition constant as defined in eq 4. k_{basal} is the rate in the absence of monovalent cation.

The IMPDH Reaction in the Absence of K^+. The steady-state kinetic parameters were determined in the absence of monovalent cations (Table 1). Ionic strength was maintained with tetramethylammonium chloride, which neither activated nor inhibited *Cp*IMPDH. Strong NAD^+ substrate inhibition was observed under these conditions. Therefore, we also characterized the reaction at 1 mM K^+, where NAD^+ inhibition was less severe, and with acetylpyridine adenine dinucleotide ($APAD^+$), a NAD^+ analogue that did not display substrate inhibition.

As expected, the values of k_{cat} for the reaction of both NAD^+ and $APAD^+$ decreased by a factor of 10–20 in the absence of K^+. While the values of K_m for IMP and $APAD^+$ did not change, the value of $K_m(NAD^+)$ increased and the value of $K_{ii}(NAD^+)$ decreased in the absence of K^+. These opposing actions suggested that K^+ increased the affinity of NAD^+ for E·IMP but decreased its affinity for E-XMP*.

Substrate and Product Binding in the Absence of K^+. The affinity of substrates/products/inhibitors for *Cp*IMPDH was measured by monitoring changes in intrinsic protein fluorescence. Simple hyperbolic binding curves were observed in all cases (Table 2 and Figure S2). The values of K_d were K^+-independent for IMP, XMP, GMP, NAD^+, and NADH. These observations suggested that either K^+ did not bind to the binary enzyme–substrate complexes or substrates bound with equal affinity to both E and E·K^+. Similar observations have been made with IMPDHs from other sources.[16,17]

Unfortunately, the K^+ dependence of the kinetics of IMP, NAD^+, and XMP binding could not be determined because all of the reactions were complete within the mixing time of the stopped-flow instrument.

K^+ Changes the Rate-Limiting Step. We next sought to identify the rate-limiting step in the absence of K^+. Since the values of k_{cat} were similar for the NAD^+ and $APAD^+$ reactions (Table 1), neither hydride transfer nor NADH release was likely to be rate-limiting. Consistent with this expectation, no isotope effect was observed on k_{cat} when 2-^{2}H-IMP was the substrate (Table 1), and a burst of NADH production was observed in the pre-steady state (Figure 4). When the reaction was performed with [8-^{14}C]-IMP and NAD^+, 43 ± 3% of

dx.doi.org/10.1021/bi200785s | *Biochemistry* 2011, 50, 8508–8518

Table 1. Steady-State and Inhibition Parameters for *Cp*IMPDH in the Presence and Absence of K^+ [a]

	no K^+		1 mM K^+	100 mM K^+	
parameter	NAD^+	$APAD^+$	NAD^+	NAD^+	$APAD^+$
k_{cat} (s^{-1})	0.27 ± 0.08[c,i]	0.16 ± 0.01[c]	0.8 ± 0.2[c]	2.6 ± 0.1[b]	3.0 ± 0.1[b]
$K_{M\ IMP}$ (μM)	10 ± 2[d]	nd[e]	nd[e]	13 ± 3[b]	nd[e]
$K_{M\ dinucleotide}$ (μM)	1400 ± 500[c]	220 ± 30[c]	2400 ± 800[c]	140 ± 10[b]	190 ± 10[b]
$K_{ii\ dinucleotide}$ (μM)	600 ± 200[c]	na[f]	1500 ± 500[c]	4900 ± 500[b]	na[f]
$^{D}k_{cat}$[g]	n.d.	1.1 ± 0.1	nd[e]	nd[e]	0.99 ± 0.05
$^{D}k_{cat}/K_M$[g]	n.d.	3.8 ± 0.2	nd[e]	nd[e]	1.15 ± 0.12
$^{H_2O}k_{cat}/^{D_2O}k_{cat}$	1.1 ± 0.4[i]	1.1 ± 0.1	nd[e]	2.6 ± 0.1[b]	3.3 ± 0.1[b]
α[h]	nd[e]	1.2 ± 0.4	0.3 ± 0.1	0.2 ± 0.04[j]	0.10 ± 0.03

[a]All experiments are at equivalent ionic strength at 25 °C. No K^+ conditions: 280 mM Tris-Cl, pH 8.0 and 1 mM DTT; 1 mM K^+ conditions: 278 mM Tris-Cl, pH 8.0, 1 mM KCl, and 1 mM DTT; 100 mM K^+ conditions: 50 mM Tris-Cl, pH 8.0, 100 mM KCl, and 1 mM DTT. [b]Values from ref 29. [c]Varying dinucleotide at 500 μM IMP. [d]Varying IMP at 900 μM NAD^+. [e]Not determined. [f]Not applicable. [g]Isotope effect with ^{2}H-IMP in the $APAD^+$ reaction. [h]Interaction constant for tiazofurin and ADP. [i]NAD^+ substrate inhibition introduces high errors into the determination of k_{cat}. [j]Value from ref 30.

Table 2. Affinities of Substrates, Products, and Inhibitor in the Presence and Absence of K^+ [a]

	K_d (μM)	
ligand	no KCl	100 mM KCl
IMP	4.6 ± 0.3	4.7 ± 0.4
NAD	20 ± 5	14 ± 1
XMP	7.1 ± 0.3	5.6 ± 0.6
NADH	2.4 ± 0.4	2.3 ± 0.2
GMP	2.4 ± 0.2	4.8 ± 0.6

[a]Determined by monitoring changes in intrinsic protein fluorescence upon ligand binding.

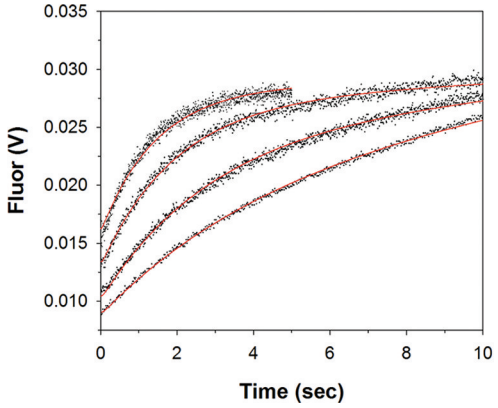

Figure 4. Pre-steady-state reaction in the absence of K^+. Progress curves for the reaction of E·IMP with 5 mM NAD^+ were measured by stopped-flow spectroscopy monitoring fluorescence at 25 °C. Final concentrations after mixing are 0.5 μM enzyme, 500 μM IMP, 280 mM Tris-Cl, pH 8.0, and 1 mM DTT [NAD^+] = 1.25, 2.5, 5.0, and 10 mM (bottom trace to top). Progress curves for the reaction monitored by absorbance can be found in the Supporting Information. Global fits of the fluorescence and absorbance data to the mechanism of Figure 1B are shown in red. The signal response coefficients (SRC) in the fluorescence data were floated to account for inner filter effects at high NAD^+ concentrations. In the worst case (10 mM NAD^+), the fitted SRC was 75% of the calculated SRC.

enzyme was trapped as E-XMP*, indicating that E-XMP* accumulated during steady state. Similarly, 53 ± 2% of the enzyme was trapped as E-XMP* in the reaction of $APAD^+$. These observations would usually indicate that the hydrolysis of E-XMP* was the slow step. However, no solvent isotope effect was observed when the reaction was performed in D_2O (Table 1). *Therefore, in the absence of K^+, neither hydride transfer, NADH release, nor the hydrolysis of E-XMP* was rate-limiting.*

K^+ Accelerates a Conformational Change. The above experiments indicated that the rate-limiting step occurred after NADH was released but before water attacked E-XMP*. Therefore, closure of the flap was the slow step, i.e., k_{closed} = 0.2 s^{-1}, and E-XMP*$_{open}$ was the major enzyme form. The severe NAD^+ substrate inhibition supported this conclusion: if more E-XMP*$_{open}$ was present, then the E-XMP*·NAD^+ complex would form more readily.

Unfortunately, the value of k_{closed} has not been measured in the presence of K^+. However, since a solvent isotope effect is observed in the presence of K^+, the value of k_{closed} must be ≥13 s^{-1}. Therefore, the presence of K^+ increased the value of k_{closed} by at least a factor of 65.

Flap closure can be probed with a double inhibitor experiment (explained in detail in the Supporting Information).[29,31,37,38] In brief, tiazofurin binds in the nicotinamide half of the dinucleotide site while ADP binds in the adenosine subsite. These inhibitors are intrinsically independent, so if the open conformation predominates, the interaction constant α will be ~1.[31] However, if the closed conformation predominates, then tiazofurin will pull the equilibrium toward the open conformation, facilitating the binding of ADP, and a synergistic interaction will be observed with $\alpha \leq 1$. We performed this experiment with $APAD^+$ to avoid complications with NAD^+ substrate inhibition.

In the presence of 100 mM K^+, the two inhibitors were indeed strongly synergistic, with an interaction constant α = 0.10 ± 0.03 in the $APAD^+$ reaction. This value agreed well with that previously determined with NAD^+ (α = 0.20 ± 0.04[30]). Therefore, the value of K_c is 4–9 in the presence of 100 mM K^+. In contrast, the two inhibitors were independent in the absence of K^+ (α = 1.2 ± 0.3; Figure S3). This observation indicated that E-XMP*$_{open}$ was the predominant enzyme form, as expected if the conformational change was slow. Overall, the data were reasonably self-consistent: if the fraction of E-XMP*$_{open}$ increased from 20% to 100% in the absence of K^+, then the value of K_{ii} for NAD^+ should decrease to 300 μM, in fair agreement with experiment (K_{ii} = 600 μM).

dx.doi.org/10.1021/bi200785s | *Biochemistry* 2011, 50, 8508–8518

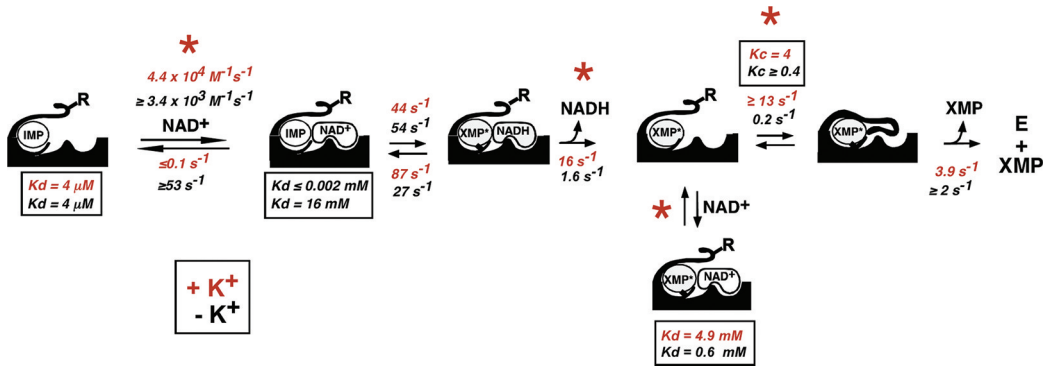

Figure 5. Kinetic mechanism of *Cp*IMPDH in the presence and absence of K^+. The mechanism in the presence of K^+ is from ref 29. The kinetic and binding parameters are shown in orange for the reaction in the presence of 100 mM K^+ and black for the reaction in the absence of K^+. Orange stars mark the K^+-dependent steps.

Unfortunately, since flap closure was rate-limiting, the value of K_c in the absence of K^+ cannot be estimated. A lower limit $K_c \geq 0.4$ can be established from the constraint that no solvent isotope effect was observed (see Table S2). Therefore, K^+ stabilized the closed conformation by no more than a factor of 20 ($\leq$1.8 kcal/mol). A value of $K_c \sim 2-4$ was determined at 1 mM K^+. These findings suggested that K^+ had a larger effect on the kinetics of the conformational change than on the equilibrium between E-XMP*$_{open}$ and E-XMP*$_{closed}$.

The Kinetic Mechanism of CpIMPDH in the Absence of K^+. We derived rate constants for each step of the IMPDH reaction in the absence of K^+ by globally fitting the pre-steady-state reaction progress curves using Dynafit[39] and applying the constraints from the steady-state data (Figures 4 and 5; see Supporting Information for a detailed description as well as Figures S4 and S5 and Tables S1 and S2). Surprisingly, although the crystal structures imply that K^+ stabilized E-XMP*, neither chemical transformation was significantly K^+-dependent. In contrast, the NAD(H) binding steps displayed strong dependence on K^+. The largest effect was on the affinity of NAD^+ for E·IMP, which decreased by a factor of 10^4 in the absence of K^+. Likewise, the rate constant for the release of NADH was lower by a factor of ~10. These observations indicated that K^+ was present throughout the catalytic cycle. Therefore, X-ray crystal structures that do not include K^+ are unlikely to be catalytically relevant.

Molecular Dynamics Models. Crystal structures of E-XMP*$_{open}$ and E-XMP*$_{closed}$ do not exist, so we performed free energy simulations to provide insight into how K^+ influences the structure of the open and closed conformations. The alchemical free energy simulations were performed based on the orthogonal space random walk (OSRW) strategy implemented in a customized version of the CHARMM program.[34,35,40] As discussed in Methods and Materials, this technique was enabled with adaptive updates of two biasing energy terms, one of which is the function of the generalized force (the orthogonal space biasing term). With this specialized biasing potential treatment, this technique allows quantitative free energy simulations to be realized when structural changes are strongly coupled to chemical transitions.

Since the K^+ site and flap are disordered in the X-ray crystal structure of *Cp*IMPDH, we constructed models based on X-ray crystal structures of *Tf*IMPDH.[12,14,15] Models were constructed with the program Modeler[41] (coordinates are available from the authors upon request). The models included a single monovalent cation site and the corresponding two IMPDH monomers. The Cys319 loop and C-terminal segment of *Cp*IMPDH are 60% and 22% identical to the analogous regions of *Tf*IMPDH, respectively (Table S4; *Tf* IMPDH numbering will be used throughout for clarity). Protein atoms >35 Å from the K^+ site were fixed to retain the overall structural integrity (Figure 6A). All water molecules were dynamically simulated.

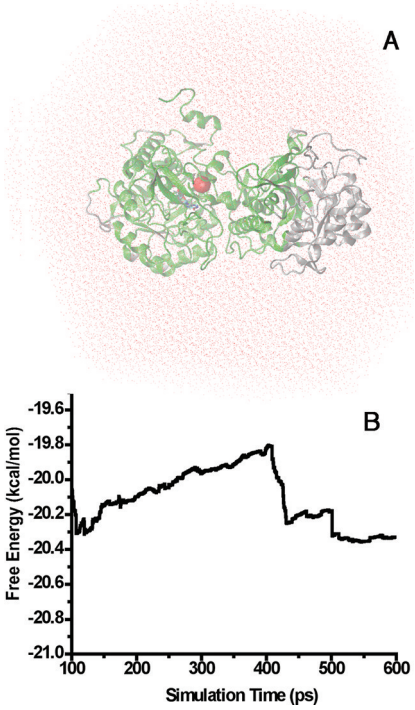

Figure 6. Computational models of *Cp*IMPDH. (A) Two monomers and the associated K^+ (red ball) were modeled based on *Tf*IMPDH (1PVN) with a truncated octahedral water box. All water molecules are dynamic (red dots), but residues >35 Å from the K^+ site were fixed (colored gray); yellow, β-sheet; magenta, α-helix; blue, loop. (B) Free energy convergence as illustrated in the change of Na^+ into K^+. The temperature was set as 300 K, which was kept constant via the Langevin thermostat. Molecular dynamics simulations were integrated via a time-step of 1 fs.

The E-XMP*$_{closed}$ conformation of *Cp*IMPDH was modeled based on the structure of the E·MZP·K^+ complex of *Tf*IMPDH, where the flap occupies the dinucleotide site and is completely ordered (1PVN). The MZP ligand was replaced with the XMP* intermediate. The flap of *Cp*IMPDH contains four more

dx.doi.org/10.1021/bi200785s | *Biochemistry* 2011, 50, 8508–8518

residues than *Tf*IMPDH; this segment was built by fixing the backbone positions of the aligned residues, and an OSRW-based accelerated MD simulation, which focussed on the sampling of the flap region was performed to relax the new residues.[35]

The Simulations Recapitulate Cation Selectivity. The binding of *Cp*IMPDH to various monovalent cations was simulated in order to validate the model. As described earlier, in each of binding simulations, a scaling parameter λ was used to switch the state from one ion to another; e.g., when $\lambda = 0$, the state is Na^+, and when $\lambda = 1$, the state is K^+. Figure 6B shows the example of the transition between K^+ and Na^+ in the E-XMP*$_{closed}$ model; convergence is obtained with a fluctuation range of about 0.1 kcal/mol in 500 ps simulations. It would be impossible to realize such fast convergence in a system of this size with typical computational resources without the OSRW technique.

K^+ interacted with the same six carbonyl oxygens in the Cys319 loop and C-terminal segment as observed in *Tf*IMPDH (Table 3 and Figure 7A). Similar affinity and virtually identical interactions were observed with NH_4^+, as expected given the similar sizes of these two cations (Figure 7B). Thus, the simulations accounted for the ability of K^+ and NH_4^+ to activate *Cp*IMPDH. A very different situation was revealed when we interrogated the binding of other cations to *Cp*IMPDH, in keeping with the experimental observations described above. Na^+, Mg^{2+}, and Ca^{2+} had lower affinity for E-XMP*$_{closed}$ than K^+ (Table 3; note that the relative binding affinity between K^+ and another ion was calculated based on $\Delta G_{(ion\rightarrow K/closed)} - \Delta G_{(ion\rightarrow K/bulk\ water)}$, where $\Delta G_{(ion\rightarrow K/closed)}$ and $\Delta G_{(ion\rightarrow K/bulk\ water)}$ were directly calculated by two corresponding alchemical free energy simulations respectively in the protein environment and the aqueous solution). Moreover, these ions made very different interactions with the protein. In the simulations of Na^+ binding, only four carbonyls interacted with the smaller Na^+ ion (Figure 7C). Importantly, the interaction with Cys319 was lost. Similar results were observed with Mg^{2+} and Ca^{2+} (Figure 7D and Figure S6); the even smaller Mg^{2+} ion also interacted with only four carbonyls while a much looser binding site formed to accommodate Ca^{2+}. Though the coordination structures resulting from the treatment of divalent cations with nonpolarizable force fields can be uncertain,[42] nonetheless these simulations provided further validation for the homology model.

Table 3. Relative Free Energies of Monovalent Cation Binding to the E-XMP*$_{closed}$ Estimated from Alchemical Free Energy Calculations[a]

cation	$\Delta\Delta G$ (kcal/mol)	cation	$\Delta\Delta G$ (kcal/mol)
K^+	0	Na^+	1.6
dummy ion	1.5[b]	Ca^{2+}	7.2
NH_4^+	−0.9	Mg^{2+}	8.8

[a]The relative free energies of monovalent cation binding are calculated with the K^+ binding state as the reference in the corresponding alchemical free energy calculations. [b]$\Delta\Delta G$ is the absolute energy of the no-ion state to the K^+ binding state in 100 mM solution; i.e., the absolute binding affinity of K^+ is estimated based on eq 5 with [ion] = 100 mM.

K^+ Mobilizes Residues 318−320 To Facilitate Flap Closure. The absence of K^+ was simulated with a dummy particle that did not interact with the other atoms but was restrained to interact with the carbonyl oxygen of residue 314. The binding affinity of K^+ was calculated based on $\Delta G_{(dummy\rightarrow K/closed)} - \Delta G_{(dummy\rightarrow K/bulk\ water)} + \Delta G_{restraint}$, where $\Delta G_{(dummy\rightarrow K/closed)}$ and $\Delta G_{(dummy\rightarrow K/bulk\ water)}$ were directly calculated by two alchemical free energy simulations respectively in the protein environment and the aqueous solution and $\Delta G_{restraint}$ was estimated based on eq 5. The result indicated that K^+ stabilizes E-XMP*$_{closed}$ by 1.5 kcal/mol in the presence of 100 mM K^+ (Table 3).

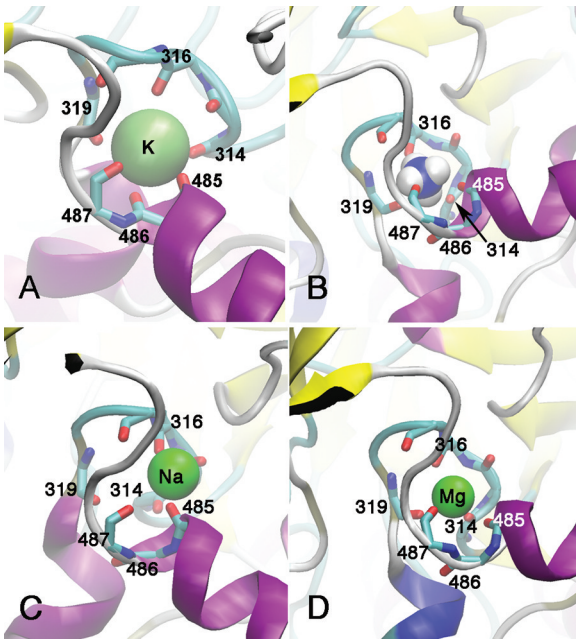

Figure 7. Models of ion binding in *Cp*IMPDH resulting from the corresponding OSRW MD simulations. (A) K^+ interacts with six carbonyl oxygens from residues 314, 316, 319 (the catalytic Cys), 485, 486, and 487 as observed in *Tf*IMPDH. (B) NH_4^+ makes the same interactions as K^+, accounting for its similar ability to activate *Cp*IMPDH. (C) The smaller Na^+ ion interacts with only four carbonyl oxygens, 314, 316, 485, and 487, thus accounting for its inability to activate *Cp*IMPDH. (D) Mg^{2+} also interacts with only four carbonyls.

These simulations also revealed changes in the interactions between the Cys319 loop and flap that could explain how K^+ controlled flap closure. In the absence of K^+, the backbone carbonyl of Cys319 rotated away from the ion binding site and the local secondary structure relaxed (Figure 9A). Residues 318−320 became more linear, and the adjacent helix became more ordered. The carbonyl of residue 320 formed a hydrogen bond to the NH of residue 324, which created one turn of α-helix. This finding was corroborated by the X-ray crystal structure of IMPDH from *Borrelia burgdorferi* (*Bb*IMPDH; 1EEP), which has the identical Cys319 loop sequence as *Cp*IMPDH; this complex does not contain K^+, and residues 319−325 form two turns of an α-helix (Figure S7A).[43] We propose that this more ordered structure hinders flap motion. K^+-binding mobilizes residues 318−320, which permits the formation of hydrogen bonds between the Cys319 loop and the hinge region of the flap (Figure 8A). We further propose that these interactions play a critical role in facilitating the flap closure.

The Association of K^+ with the Open Conformation. To probe the binding of K^+ to E-XMP*$_{open}$, we also constructed a model of *Cp*IMPDH based on structure 1ME7, where Na^+ occupies the conserved monovalent cation site, ribavirin

dx.doi.org/10.1021/bi200785s | *Biochemistry* 2011, 50, 8508−8518

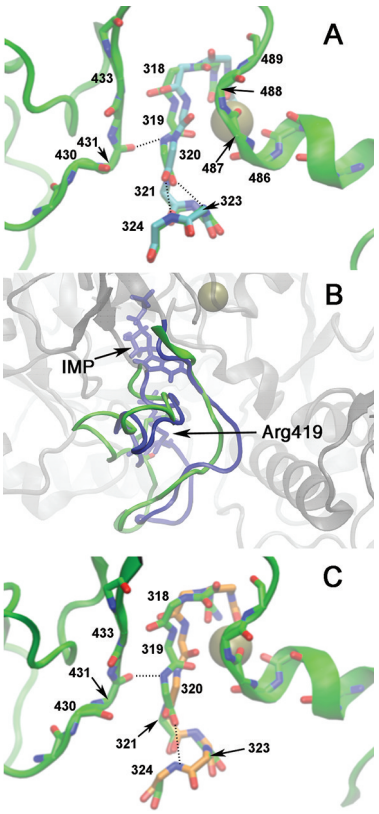

Figure 8. Structural changes associated with K^+ binding in *Cp*IMPDH. Models were constructed based on structures of *Tf*IMPDH, 1PVN (E·MZP·K^+ complex, a model for E-XMP*$_{closed}$), and 1ME7 (E·RVP·MPA·Na^+ complex, leading to E-XMP*$_{open}$ model). *Tf*IMPDH numbering is used to enable ready comparison with Figure 2. The corresponding residues are Ile218, Cys219, Thr220, Ile323, Val324, Arg315, Glu329, Ile331, Glu383, Ser384, His385, and Asp386 in *Cp*IMPDH. (A) Models of K^+ binding site and the flap hinge region of E-XMP*$_{closed}$ with K^+ (green) and with the dummy ion (cyan). (B) The different conformations of the flap in the E-XMP*$_{closed}$ model (blue) and the E-XMP*$_{open}$ model (green). XMP* (sticks), K^+ (gold sphere), and the catalytic Arg (sticks) are shown. (C) The structures of the K^+-bound form of E-XMP*$_{closed}$ (green) and E-XMP*$_{open}$ model (orange).

monophosphate binds in the IMP site, and mycophenolic acid binds in the NAD site of *Tf*IMPDH. This structure has several significant differences relative to 1PVN: (1) the C-terminal segment forms a loose helix where the residues are too far apart to form the canonical $n/n + 4$ hydrogen bonds (Figure S7B); (2) the Cys319 loop has shifted and the helical segment is looser than in 1PVN; and (3) flap residues 417−430 are disordered. As above, the ligands were replaced with the XMP* intermediate, and the missing segment was built based on the structural superimposition and OSRW accelerated simulation refinement. The enzyme assumed a conformation that has not been observed in a crystal structure, wherein the flap interacts with the barrel domain but Arg419 remains outside the active site (Figure 8B). Therefore, this conformation is not competent to perform the hydrolysis reaction. The Cys319 loop also assumed a novel conformation that is intermediate between the conformations observed in the E-XMP*$_{closed}$ and E-XMP*$_{closed}$·K^+, where the backbone carbonyl of Cys319 interacted with K^+ and a hydrogen bond formed between residues 318 and 433′. In addition, the carbonyl of residue 320 formed a hydrogen bond with residue 324 as in E-XMP*$_{closed}$; this helix was distorted in E-XMP*$_{closed}$·K^+ (Figure 8C).

As above, we used the OSRW method to interrogate the affinity and specificity of monovalent cation binding to E-XMP*$_{open}$. The simulations indicated that E-XMP*$_{open}$ had a higher affinity for K^+ than E-XMP*$_{closed}$ (Table 3). This higher affinity might be explained by the more stable secondary structure of the Cys319 loop. E-XMP*$_{open}$ also had a stronger preference for K^+ over Na^+ ($\Delta\Delta G$ = −2.8 kcal/mol). Thus, these simulations suggested that K^+ stabilized an enzyme conformation that was not competent to perform the hydrolysis reaction.

K^+ Loosens the Closed Conformation of the Flap.

Potential of mean force calculations were performed to understand how K^+ influences the E-XMP*$_{closed}$. The average of the distances between each C-α atom in the flap and the center of the purine base in E-XMP* was employed as the collective variable; the smaller this collective variable, the more closed the flap is. For comparison, the collective variable for the closed conformation found in 1PVN is 13 Å. Each of the free energy potentials was obtained with the collective variable reaching a round-trip random walk in the range 12−17 Å (Figure 9); note that the state with the collective variable value

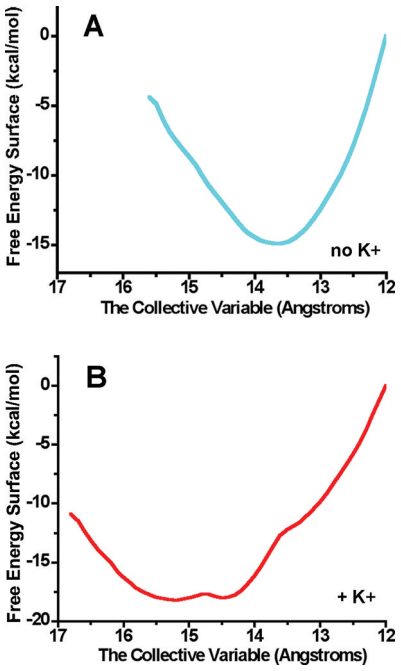

Figure 9. Potential of mean force experiments. (A) Calculation for the closed conformation in the absence of K^+. (B) Calculation for the closed conformation in the presence of K^+.

of 12.0 Å was used as the reference point, so the absolute energy values of panels A and B are not directly comparable).

A narrow energy well was observed in the absence of K^+, with a free energy minimum at ∼14 Å (Figure 9A). This calculation suggested that a significant barrier existed between the open and closed conformations. In contrast, when K^+ was present, a broad energy well was observed with a minimum at ∼15 Å (Figure 9B). Thus, the presence of K^+ moved the position of the closed conformation toward the open state, making conformational exchange more facile.

dx.doi.org/10.1021/bi200785s | *Biochemistry* 2011, 50, 8508−8518

DISCUSSION

Impact of K^+ on the CpIMPDH Reaction. One clear conclusion of these experiments is that monovalent cations must bind concomitantly with NAD^+ and be present during the remainder of the catalytic cycle. Similar kinetic mechanisms have been proposed for IMPDHs from *Aerobacter aerogenes*, *Escherichia coli*, and humans based on steady-state kinetic experiments.[17,19,27] Unfortunately, none of the IMPDH structures containing NAD^+ or its analogue TAD also contain monovalent cations, so these structures are unreliable mimics of catalytically competent complexes.

Although the value of k_{cat} is K^+-dependent, K^+ does not accelerate either chemical transformation. Instead, K^+ accelerates the formation of E-XMP*$_{closed}$, in effect activating *Cp*IMPDH by catalyzing protein motion. Intriguingly, it is possible that the K^+ dependence of the dinucleotide binding steps also derives from the acceleration of protein conformational changes. The Callender laboratory has shown that the association of NADH to lactate dehydrogenase involves at least three conformational rearrangements after formation of the initial encounter complex, and subsequent binding of lactate requires two conformational changes.[44,45] Analogous conformational changes are surely required for the association/dissociation of substrates to IMPDH.

How Does K^+ Promote Protein Motion? K^+ interacts with main chain carbonyls of the Cys319 loop and the C-terminal segment in IMPDH. The simulations suggest that the structure of the Cys319 loop relaxes back into a more stable secondary structure in the absence of K^+. The binding of K^+ provides alternative interactions for the carbonyl groups. This structural mobilization permits interactions between the Cys319 loop and the flap, which in turn facilitate closure. We have recently demonstrated that mutations in loop residues 322−324 perturb flap closure in *Tf*IMPDH, further validating this mechanism.[26] Intriguingly, the carboxamide oxygens of NAD^+ and TAD interact with the amide nitrogen of residue 314 in several crystal structures. In these conformations of the Cys319 loop, the carbonyl of residue 314 is displaced ∼3 Å from its position in the K^+ binding site of E-XMP*. Perhaps the K^+ dependence of dinucleotide binding involves an analogous mobilization of residue 314 via competing interactions.

Kinetic versus Thermodynamic Control. Figure 10 summarizes the effects of K^+ on the equilibrium between E-XMP*$_{open}$ and E-XMP*$_{closed}$ derived from both the kinetics and computational experiments. Our best estimate for the value of $\Delta\Delta G_{eq}(\pm K^+)$ was 1.1−1.5 kcal/mol. In contrast, the effect of K^+ on the barrier to flap closure, $\Delta\Delta G^{\dagger}(\pm K^+)$, was ≥2.4 kcal/mol. Thus, the effect of K^+ on the kinetics of the conformational change exceeded the effect on the conformational equilibrium.

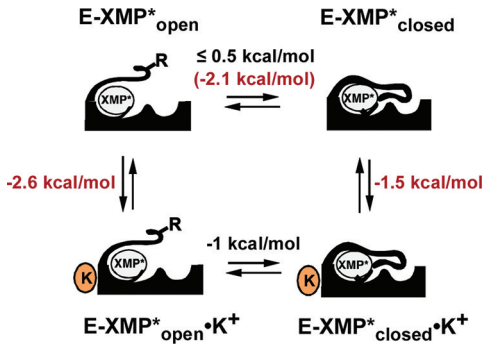

Figure 10. Interaction of K^+ with open and closed conformations of E-XMP*. Energy values are calculated for a standard state of 0.1 M K^+ as was used in the experiments. Values derived from experiments are shown in black numbers. Values derived from simulations are shown in red. Values in parentheses are calculated from the combination of experimental and computational values.

Flap closure is in essence a protein folding event, and the ratio of $\Delta\Delta G^{\dagger}(\pm K^+)/\Delta\Delta G_{eq}(\pm K^+)$ is analogous to a ϕ value, which is widely used to analyze the structure of transition states during protein folding.[46−48] Canonical ϕ values range between 0 and 1, but in our case, $\Delta\Delta G^{\dagger}(\pm K^+)/\Delta\Delta G_{eq}(\pm K^+)$ is >1.6.

Dill has suggested that such noncanonical values can result from multiple pathway folding landscapes, where the mutation blocks the fast pathway, forcing folding to proceed via a slow pathway.[49] Our simulations suggested that a similar mechanism is at play here. In the absence of K^+, the closed conformation was in a steep energy minimum. In contrast, the closed conformation was looser in the presence of K^+, with an energy minimum that is closer to the open state. Such compression of the reaction coordinate reduces reorganization energy λ and will therefore accelerate the reaction even if the conformational equilibrium is unchanged (Figure 11).

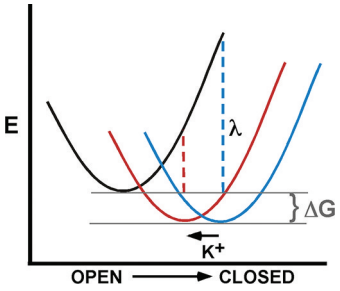

Figure 11. Allosteric activation of IMPDH by monovalent cations. K^+ preorganizes protein so that fewer structural changes are required to change from the open to closed conformation. This reaction coordinate shift has a relatively small effect on the equilibrium between open and closed conformations, but a large effect on the activation energy $\Delta G^* = (\Delta G + \lambda)^2/4\lambda$ (here, the symbol λ stands for the reorganization energy rather than the scaling parameter as used in the earlier alchemical free energy calculations).

K^+ Acts as a Ball and Socket Joint. Our results suggest the following model for K^+ activation of IMPDH. The C-terminal helix is disordered in the absence of K^+, which allows the Cys319 loop to assume a conformation that is not compatible with conformational exchange. The presence of K^+ preorganizes these regions, shrinking the reaction coordinate, thereby decreasing the activation barrier for flap closure. In effect, K^+ serves as a ball and socket joint, organizing the Cys319 loop and the C-terminal segment and accelerating the enslaved conformational transitions. Interestingly, a similar mechanism has been proposed to explain why water and salt increase enzyme activity in organic solvents.[50] Likewise, specifically bound water molecules are believed to mediate structural transitions in ribozyme catalysis.[51] The perplexing activation of P450cam by K^+ may also be an example of this phenomenon: K^+ increases the association of P450cam with putiredoxin, yet putiredoxin displaces K^+.[52] Monovalent cation activation is a widespread phenomenon,[4] so it seems likely that similar kinetic regulation of allosteric activation will be observed

dx.doi.org/10.1021/bi200785s | *Biochemistry* 2011, 50, 8508−8518

in other enzymes and perhaps even with other allosteric effectors.

Summary. IMPDH suggests a new paradigm of allosteric regulation via the kinetic control of protein conformation. K^+ appears to act as a ball and socket joint, both organizing and mobilizing structure to facilitate conformational changes. Given the prevalence of monovalent cation activation, this phenomenon may be widespread. Importantly, similar kinetically controlled allosteric mechanisms could apply to other effectors.

■ ASSOCIATED CONTENT

Supporting Information

A description of ligand binding assays, the determination of K_d, figures showing the global fits, alignments of the Cys319 loop and C-terminal segment, figures of Ca^{2+} binding model and graphics depictions of the Cys319 loop and adjacent regions, and the OSRW command file. This material is available free of charge via the Internet at http://pubs.acs.org.

■ AUTHOR INFORMATION

Corresponding Author

*Phone 781-736-2233. Fax 781-736-2349. E-mail hedstrom@brandeis.edu (L.H.); yyang2@fsu.edu (W.Y.).

Present Address

#Sirtris Pharmaceuticals, a GSK Co., 200 Technology Square, Suite 300, Cambridge, MA 02139.

Funding

This work was supported by NIH grant GM054403 (L.H.). Molecular graphics images in Figure 2 and Figure S7 were produced using the UCSF Chimera package from the Resource for Biocomputing, Visualization, and Informatics at the University of California, San Francisco (supported by NIH P41 RR001081).

■ ACKNOWLEDGMENTS

The authors thank Adrian Whitty for comments on the manuscript.

■ ABBREVIATIONS

2-Cl-IMP, 2-chloroinosine 5′-monophosphate; 6-Cl-PRT, 6-Cl-purine ribotide; $APAD^+$, acetylpyridine adenine dinucleotide; IMP, inosine 5′-monophosphate; IMPDH, IMP dehydrogenase; MPA, mycophenolic acid; RVP, ribavirin 5′-monphosphate; XMP, xanthosine 5′-monophosphate.

■ REFERENCES

(1) Pauling, L. (1935) The oxygen equilibrium of hemoglobin and its structural interpretation. *Proc. Natl. Acad. Sci. U. S. A. 21*, 181−191.

(2) Monod, J., Wyman, J., and Changeux, J. P. (1965) On the natue of allosteric transitions: a plausible model. *J. Mol. Biol. 12*, 88−118.

(3) Koshland, D. E., Nemethy, G., and Filmer, D. (1966) Comparison of experimental binding data and theoretical models in proteins containing subunits. *Biochemistry 5*, 365−385.

(4) Page, M. J., and Di Cera, E. (2006) Role of Na+ and K+ in enzyme function. *Physiol. Rev. 86*, 1049−1092.

(5) Cui, Q., and Karplus, M. (2008) Allostery and cooperativity revisited. *Protein Sci. 17*, 1295−1307.

(6) Goodey, N. M., and Benkovic, S. J. (2008) Allosteric regulation and catalysis emerge via a common route. *Nat. Chem. Biol. 4*, 474−482.

(7) Swain, J. F., and Gierasch, L. M. (2006) The changing landscape of protein allostery. *Curr. Opin. Struct. Biol. 16*, 102−108.

(8) del Sol, A., Tsai, C. J., Ma, B. Y., and Nussinov, R. (2009) The Origin of Allosteric Functional Modulation: Multiple Pre-existing Pathways. *Structure 17*, 1042−1050.

(9) Cooper, A., and Dryden, D. T. (1984) Allostery without conformational change. A plausible model. *Eur. Biophys. J. 11*, 103−109.

(10) Popovych, N., Sun, S., Ebright, R. H., and Kalodimos, C. G. (2006) Dynamically driven protein allostery. *Nat. Struct. Mol. Biol. 13*, 831−838.

(11) Toncrova, H., and McLeish, T. C. (2010) Substrate-modulated thermal fluctuations affect long-range allosteric signaling in protein homodimers: exemplified in CAP. *Biophys. J. 98*, 2317−2326.

(12) Hedstrom, L. (2009) IMP Dehydrogenase: structure, mechanism and inhibition. *Chem. Rev. 109*, 2903−2928.

(13) Sintchak, M. D., Fleming, M. A., Futer, O., Raybuck, S. A., Chambers, S. P., Caron, P. R., Murcko, M., and Wilson, K. P. (1996) Structure and mechanism of inosine monophosphate dehydrogenase in complex with the immunosuppressant mycophenolic acid. *Cell 85*, 921−930.

(14) Prosise, G. L., Wu, J. Z., and Luecke, H. (2002) Crystal Structure of Tritrichomonas foetus Inosine Monophosphate Dehydrogenase in Complex with the Inhibitor Ribavirin Monophosphate Reveals a Catalysis-dependent Ion-binding Site. *J. Biol. Chem. 277*, 50654−50659.

(15) Gan, L., Seyedsayamdost, M. R., Shuto, S., Matsuda, A., Petsko, G. A., and Hedstrom, L. (2003) The immunosuppressive agent mizoribine monophosphate forms a transition state analog complex with IMP dehydrogenase. *Biochemistry 42*, 857−863.

(16) Markham, G. D., Bock, C. L., and Schalk-Hihi, C. (1999) Acid-base catalysis in the chemical mechanism of inosine monophosphate dehydrogenase. *Biochemistry 38*, 4433−4440.

(17) Xiang, B., Taylor, J. C., and Markham, G. D. (1996) Monovalent cation activation and kinetic mechanism of inosine 5′-monophosphate dehydrogenase. *J. Biol. Chem. 271*, 1435−1440.

(18) Colby, T. D., Vanderveen, K., Strickler, M. D., Markham, G. D., and Goldstein, B. M. (1999) Crystal structure of human type II inosine monophosphate dehydrogenase: implications for ligand binding and drug design. *Proc. Natl. Acad. Sci. U. S. A. 96*, 3531−3536.

(19) Kerr, K. M., Cahoon, M. C., Bosco, D. A., and Hedstrom, L. (2000) Monovalent cation activation in *Escherichia coli* IMP dehydrogenase. *Arch. Biochem. Biophys. 375*, 131−137.

(20) Gan, L., Petsko, G. A., and Hedstrom, L. (2002) Crystal structure of a ternary complex of Tritrichomonas foetus inosine 5′-monophosphate dehydrogenase: NAD+ orients the active site loop for catalysis. *Biochemistry 41*, 13309−13317.

(21) Prosise, G.L., and Luecke, H. (2003) Crystal Structures of Tritrichomonas foetus Inosine Monophosphate Dehydrogenase in Complex with Substrate, Cofactor and Analogs: A Structural Basis for the Random-in Ordered-out Kinetic Mechanism. *J. Mol. Biol. 326*, 517−527.

(22) Whitby, F. G., Luecke, H., Kuhn, P., Somoza, J. R., Huete-Perez, J. A., Philips, J. D., Hill, C. P., Fletterick, R. J., and Wang, C. C. (1997) Crystal structure of Tritrichomonas foetus inosine-5′-monophosphate dehydrogenase and the enzyme-product complex. *Biochemistry 36*, 10666−10674.

(23) Hedstrom, L., and Gan, L. (2006) IMP dehydrogenase: structural schizophrenia and an unusual base. *Curr. Opin. Chem. Biol. 10*, 520−525.

(24) Bruzzese, F. J., and Connelly, P. R. (1997) Allosteric properties of inosine monophosphate dehydrogenase revealed through the thermodynamics of binding of inosine 5′-monphosphate and mycophenolic acid. Temperature dependent heat capacity of binding as a signature of ligand coupled conformational equilibria. *Biochemistry 36*, 10428−10438.

(25) Nimmesgern, E., Fox, T., Fleming, M. A., and Thomson, J. A. (1996) Conformational changes and stabilization of inosine 5′-monophosphate dehydrogenase associated with ligand binding and inhibition by mycophenolic acid. *J. Biol. Chem. 271*, 19421−19427.

(26) Josephine, H. R., Ravichandran, K. R., and Hedstrom, L. (2010) The Cys319 loop modulates the transition between dehydrogenase and hydrolase conformations in IMP dehydrogenase. *Biochemistry 49*, 10674−10681.
(27) Heyde, E., Nagabhushanam, A., Vonarx, M., and Morrison, J. (1976) Studies on inosine monophosphate dehydrogenase. Steady state kinetics. *Biochim. Biophys. Acta 429*, 645−660.
(28) MacPherson, I. S., Kirubakaran, S., Gorla, S. K., Riera, T. V., D'Aquino, J. A., Zhang, M., Cuny, G. D., and Hedstrom, L. (2010) The structural basis of Cryptosporidium -specific IMP dehydrogenase inhibitor selectivity. *J. Am. Chem. Soc. 132*, 1230−1231.
(29) Riera, T. V., Wang, W., Josephine, H. R., and Hedstrom, L. (2008) A kinetic alignment of orthologous inosine-5′-monophosphate dehydrogenases. *Biochemistry 47*, 8689−8696.
(30) Umejiego, N. N., Li, C., Riera, T., Hedstrom, L., and Striepen, B. (2004) Cryptosporidium parvum IMP dehydrogenase: Identification of functional, structural and dynamic properties that can be exploited for drug design. *J. Biol. Chem. 279*, 40320−40327.
(31) Guillén Schlippe, Y. V., Riera, T. V., Seyedsayamdost, M. R., and Hedstrom, L. (2004) Substitution of the Conserved Arg-Tyr Dyad Selectively Disrupts the Hydrolysis Phase of the IMP Dehydrogenase Reaction. *Biochemistry 43*, 4511−4521.
(32) Beglov, D., and Roux, B. (1994) Finite Representation of an Infinite Bulk System - Solvent Boundary Potential for Computer-Simulations. *J. Chem. Phys. 100*, 9050−9063.
(33) Boresch, S., Tettinger, F., Leitgeb, M., and Karplus, M. (2003) Absolute binding free energies: A quantitative approach for their calculation. *J. Phys. Chem. B 107*, 9535−9551.
(34) Zheng, L., Chen, M., and Yang, W. (2008) Random walk in orthogonal space to achieve efficient free-energy simulation of complex systems. *Proc. Natl. Acad. Sci. U. S. A. 105*, 20227−20232.
(35) Zheng, L., Chen, M., and Yang, W. (2009) Simultaneous escaping of explicit and hidden free energy barriers: application of the orthogonal space random walk strategy in generalized ensemble based conformational sampling. *J. Chem. Phys. 130*, 234105.
(36) Laio, A., and Parrinello, M. (2002) Escaping free-energy minima. *Proc. Natl. Acad. Sci. U. S. A. 99*, 12562−12566.
(37) Guillén Schlippe, Y. V., and Hedstrom, L. (2005) Is Arg418 the Catalytic Base Required for the Hydrolysis Step of the IMP Dehydrogenase Reaction? *Biochemistry 44*, 11700−11707.
(38) Kohler, G. A., Gong, X., Bentink, S., Theiss, S., Pagani, G. M., Agabian, N., and Hedstrom, L. (2005) The functional basis of mycophenolic acid resistance in Candida albicans IMP dehydrogenase. *J. Biol. Chem. 280*, 11295−11302.
(39) Kuzmic, P. (1996) Program DYNAFIT for the analysis of enzyme kinetic data: application to HIV proteinase. *Anal. Biochem. 237*, 260−273.
(40) MacKerell, A. D. Jr., Bashford, D., Bellott, M., Dunbrack, R. L., Evanseck, J. D., Field, M. J., Fischer, S., Gao, J., Guo, H., Ha, S., Joseph-McCarthy, D., Kuchnir, L., Kuczera, K., Lau, F. T. K., Mattos, C., Michnick, S., Ngo, T., Nguyen, D. T., Prodhom, B., Reiher, W. E. III, Roux, B., Schlenkrich, M., Smith, J. C., Stote, R., Straub, J., Watanabe, M., Wiorkiewicz-Kuczera, J., Yin, D., and Karplus, M. (1998) All-Atom Empirical Potential for Molecular Modeling and Dynamics Studies of Proteins. *J. Phys. Chem. B 102*, 3586−3616.
(41) Eswar, N., Marti-Renom, M. A., Webb, B., Madhusudhan, M. S., Eramian, D., Shen, M., Pieper, U., and Sali, A. (2006) Comparative Protein Structure Modeling With MODELLER, in *Current Protocols in Bioinformatics* (Baxevanis, A. D., Ed.) pp 5.6.1−5.6.30, John Wiley & Sons,Inc., New York.
(42) Yu, H. B., Whitfield, T. W., Harder, E., Lamoureux, G., Vorobyov, I., Anisimov, V. M., MacKerell, A. D., and Roux, B. (2010) Simulating Monovalent and Divalent Ions in Aqueous Solution Using a Drude Polarizable Force Field. *J. Chem. Theory Comput. 6*, 774−786.
(43) McMillan, F.M., Cahoon, M., White, A., Hedstrom, L., Petsko, G. A., and Ringe, D. (2000) Crystal structure at 2.4 Å resolution of Borrelia burgdorferi Inosine 5′-monophosphate dehydrogenase: evidence of a substrate-induced hinged-lid motion by loop 6. *Biochemistry 39*, 4533−4542.
(44) Deng, H., Zhadin, N., and Callender, R. (2001) Dynamics of protein ligand binding on multiple time scales: NADH binding to lactate dehydrogenase. *Biochemistry 40*, 3767−3773.
(45) McClendon, S., Zhadin, N., and Callender, R. (2005) The approach to the Michaelis complex in lactate dehydrogenase: the substrate binding pathway. *Biophys. J. 89*, 2024−2032.
(46) Matouschek, A., Kellis, J. T. Jr., Serrano, L., and Fersht, A. R. (1989) Mapping the transition state and pathway of protein folding by protein engineering. *Nature 340*, 122−126.
(47) Raleigh, D. P., and Plaxco, K. W. (2005) The protein folding transition state: what are Phi-values really telling us? *Protein Pept Lett 12*, 117−122.
(48) Zarrine-Afsar, A., and Davidson, A. R. (2004) The analysis of protein folding kinetic data produced in protein engineering experiments. *Methods 34*, 41−50.
(49) Ozkan, S. B., Bahar, I., and Dill, K. A. (2001) Transition states and the meaning of Phi-values in protein folding kinetics. *Nat. Struct. Biol. 8*, 765−769.
(50) Eppler, R.K., Komor, R. S., Huynh, J., Dordick, J. S., Reimer, J. A., and Clark, D. S. (2006) Water dynamics and salt-activation of enzymes in organic media: mechanistic implications revealed by NMR spectroscopy. *Proc. Natl. Acad. Sci. U. S. A. 103*, 5706−5710.
(51) Rhodes, M. M., Reblova, K., Sponer, J., and Walter, N. G. (2006) Trapped water molecules are essential to structural dynamics and function of a ribozyme. *Proc. Natl. Acad. Sci. U. S. A. 103*, 13380−13385.
(52) OuYang, B., Pochapsky, S. S., Pagani, G. M., and Pochapsky, T. C. (2006) Specific effects of potassium ion binding on wild-type and L358P cytochrome P450cam. *Biochemistry 45*, 14379−14388.
(53) Pettersen, E. F., Goddard, T. D., Huang, C. C., Couch, G. S., Greenblatt, D. M., Meng, E. C., and Ferrin, T. E. (2004) UCSF Chimera- a visualization system for exploratory research and analysis. *J. Comput. Chem. 25*, 1605−1612.